Exciton Dynamics and Degradation Mechanism in TADF OLEDs Assessed by Modulated Electroluminescence Spectroscopy

B. Blülle*, S. Jenatsch*, H. Carrillo-Nuñez*, S. Züfle*, B. Ruhstaller*,+

* Fluxim AG, Winterthur, Switzerland

+ZHAW Zurich University of Applied Sciences, Switzerland

Abstract

An in-depth understanding of physical processes in OLEDs is crucial for the design and optimization of high-efficiency and long lifetime devices. Here we investigate the exciton dynamics of TADF OLEDs by combining advanced measurement techniques with an electrooptical simulation model covering the frequency-dependent charge and exciton transport coupled with dipole emission. We complement traditional impedance analysis with a novel characterization of the frequency dependent electroluminescence response and demonstrate its sensitivity to extract excitonic key parameters like decay rates and intersystem-crossing rates from a full OLED stack. Moreover we measure the lifetime of the TADF OLED upon constant current stressing and investigate the role of possible degradation mechanisms based on the full electrooptical simulation. We find that the efficiency roll-off can be attributed to exciton quenching with trapped electrons, whereas the number of trapping sites increases with increasing stressing time, resulting in a strong reduction in the current efficiency above onset.

Author Keywords

TADF OLEDs; advanced characterization; degradation analysis; device modeling; optimization

1. Introduction

Electrical small-signal analysis has been established as a powerful technique to investigate charge carrier dynamics in opto-electronic semiconductor devices like OLEDs[1]. While for OLEDs the complex impedance response is essentially determined by the dynamic processes of charge injection, transport, trapping and recombination, the excitonic processes are usually not reflected in the purely electrical impedance spectroscopy results. Since the formation of free carriers due to spontaneous exciton dissociation is negligible in OLEDs, the radiatively or non-radiatively decaying excitons do not contribute to the electrical response, but their dynamics influences the electroluminescent signal.

In analogy to the impedance transfer function

$$Z(\omega) = V_{ac}(\omega)/J_{ac}(\omega)$$

we can define two electrooptical transfer functions for the voltage-modulated electroluminescent spectrum (VMELS)

$$VMELS(\omega) = I_{EL}(\omega)/V_{ac}(\omega)$$

and the current-modulated electroluminescent spectrum (CMELS),

$$CMELS(\omega) = I_{EL}(\omega)/J_{ac}(\omega),$$

where V_{ac} is the frequency-dependent voltage modulation around a given steady-state voltage V_0, and J_{ac} and I_{EL} are the modulated current density and electroluminescent intensity, respectively[2,3]. The relationship between the transfer functions is illustrated in Figure 1. Note that two out of the three transfer functions fully describe the dynamic response, as the transfer functions relate to each other by

$$CMELS = Z \times VMELS.$$

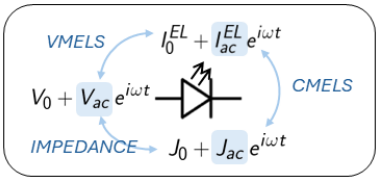

Figure 1. Illustration of the Impedance, VMELS and CMELS transfer functions describing the frequency-dependent electrical and optical OLED response.

In this contribution we employ the combination of impedance and CMELS measurements to characterize TADF OLEDs. The complex dynamic response is fitted and analyzed using the simulation software Setfos, which features full drift-diffusion charge transport modeling in steady-state, time- and frequency domain, including a rate-equation model describing the exciton dynamics and a thin-film-emission model to simulate the light generation and outcoupling.

Although the dynamic electrooptical response of an OLED in frequency-domain is fully equivalent to the response in time-domain, the frequency domain representation has particular advantages in terms of computation cost to solve the numerical system. In the small signal regime used to characterize the impedance and MELS response, the drift-diffusion and exciton equations can be linearized around the steady-state solution. This allows for a very efficient computation compared to solving the full transient problem. All impedance and MELS simulations discussed in the following were computed on an ordinary desktop computer and the data fitting was performed using Levenberg-Marquardt-based optimization routines embedded in Setfos.

2. Measured and modeled AC response of TADF OLEDs

To demonstrate the advantages of a combined steady-state and frequency-domain characterization, we have analyzed a series of four TADF OLED samples with systematically varied ETL and HTL thicknesses. Figure 1a) shows the OLED stack with the indicated HOMO/LUMO energy levels from literature. The four sample configurations are shown in Fig. 1b). We note that for parameter extraction using a model fitting approach, the

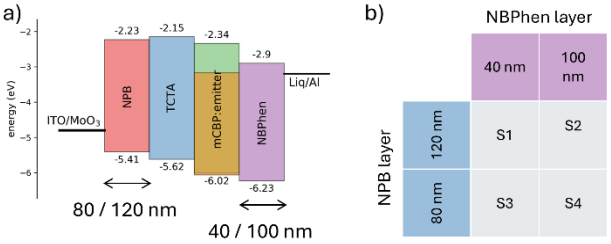

Figure 2. a) Device structure of the TADF OLEDs. b) Variation of NPB and NBPhen layer thicknesses in Samples 1 – 4

ISSN 0097-996X/25/5603-2268-$1.00 © 2025

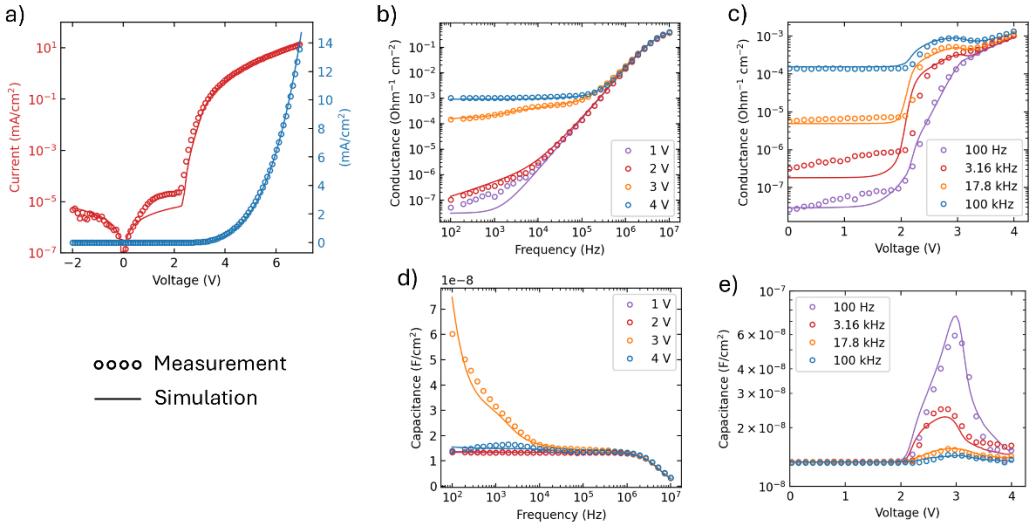

Figure 3. Measured and modeled steady-state (a) and impedance characteristics (b-e) of TADF sample S1. The impedance results are expressed in terms of conductance (b) and capacitance spectrum (d) and conductance-voltage (c) and capacitance-voltage (e).

simultaneous fitting of measurement data from multiple different sample configurations significantly lowers parameter correlations and increases the overall model reliability.

The OLEDs were characterized using Fluxim's measurement instrument Paios which features a broad variety of state-of-the-art characterization techniques in the steady-state, time- and frequency domain. In the following we focus on the analysis of the steady-state JVL characteristics in combination with Impedance spectroscopy (IS) and MELS.

In the first step, the full set of JVL and IS measurement results is replicated with Setfos 5.5, starting from a basic device stack (Fig. 2) with known layer thicknesses, energy levels from literature, and a first guess for unknown model parameters like injection barriers and electron-/hole mobilities. Following the procedure described in detail in reference [4], the model was then systematically refined, to obtain a global agreement between model and measurement.

Figure 3 shows the measured steady-state and frequency-domain response of sample 1, representative for the set of four devices, together with the model results simulated with Setfos. Here, the complex impedance response is expressed in terms of conductance and capacitance as a function of the frequency and bias voltage. A remarkable overall agreement is achieved for the full dataset, reproducing both, the bias-dependency, as well as the dynamic frequency response, including the characteristic capacitance increase at low frequencies for intermediate bias voltages. For a detailed discussion of how individual features can be attributed to physical processes we refer to [4].

In a second step we analyze the dynamics of the measured electroluminescence in response to the applied AC voltage. Figure 4 shows the frequency-dependent phases of the voltage (reference phase of 0°), the current, and the EL signal. With increasing frequency, the phase of the AC current goes ahead of the applied AC voltage, approaching a 90° phase shift before decreasing again at MHz frequencies due to the presence of a finite series resistance at the device contacts. This is in full consistency with the modeled phase for the impedance obtained from the device simulations discussed above (solid line). The electroluminescent signal, on the other hand, lags the applied AC voltage, exhibiting a characteristic phase minimum around 100 kHz.

Noteworthy, the phase shift of the EL signal is significantly larger than the one of the modeled Langevin recombination, which is considered the source of exciton generation. This difference can be directly attributed to the finite lifetime of the excitons in the TADF emitter. Indeed, from the OLED simulations in Setfos we find that solely by considering the full exciton dynamics of the TADF molecule, the modeled phase shift of the EL signal can be brought to agreement with the MELS measurement (EL curve (2) in Figure 4). For reference, curve (1) shows the modeled MELS dynamics assuming only singlet excitation without delayed fluorescence.

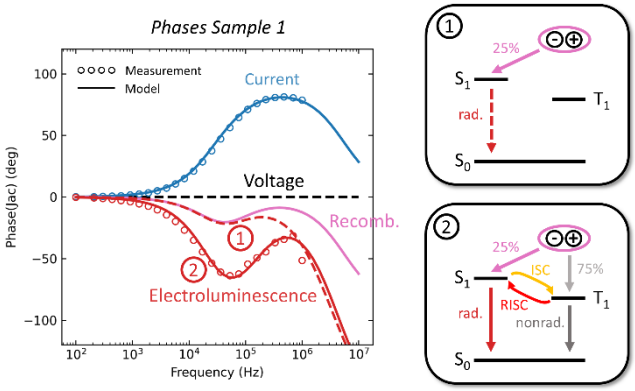

Figure 4. Measured and modeled phase shift of the current and the electroluminescent signal (VMELS transfer function) with respect to the applied AC voltage. The dashed and solid red line, respectively, show the simulated MELS dynamics for (1) a fluorescent emitter with a radiative decay channel and (2) for a TADF system featuring singlet and triplet generation including (reverse) intersystem crossing dynamics and non-radiative decay.

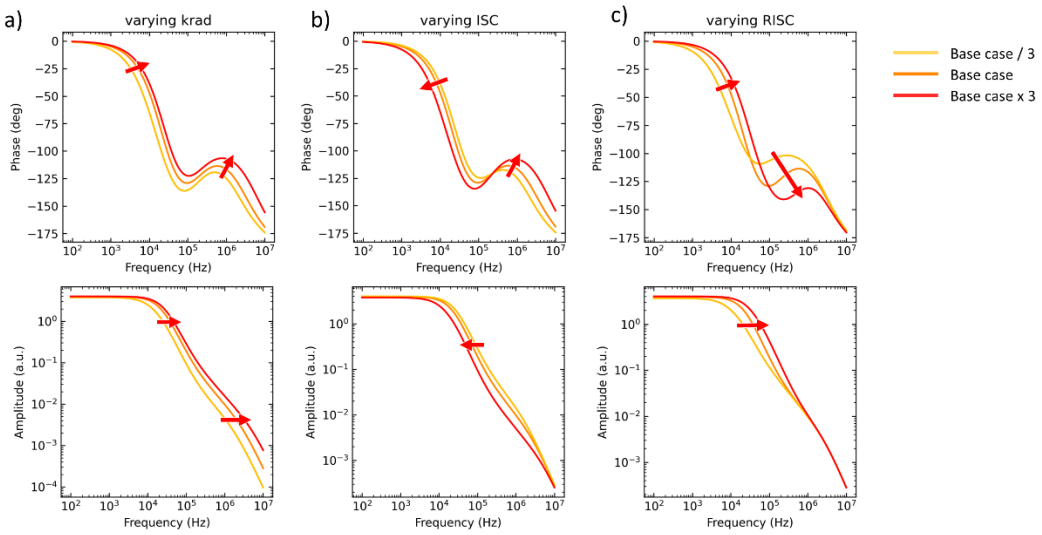

Figure 5. Modeled influence of the radiative decay rate (a), the inter-system crossing rate (b) and the reverse intersystem crossing rate (c) on the phase (top row) and the amplitude (bottom row) of the CMELS transfer function. The base case was simulated using the best fit parameters and increased / decreased by a factor of 3 to highlight that each of the exciton parameters has a distinct impact on the spectral MELS characteristics.

To illustrate the sensitivity of the MELS response to the individual excitonic parameters of the TADF system, Figure 5 shows the influence of the radiative decay rate, the intersystem-crossing (ISC) rate, and the reverse intersystem-crossing (RISC) rate on the modeled MELS phase and amplitude. For this purpose, the base values (see best fit parameters below) were increased and decreased by a factor of 3, respectively. While an increasing radiative decay rate shifts both, EL phase increase and amplitude decay towards higher frequencies, a variation of ISC and RISC, both modify the phase and amplitude at higher frequencies (> 100 MHz) in a different direction than in the lower frequency regime.

Given the distinct influence of each of these exciton parameters, it is possible to obtain a unique parameter set from a fit of the Setfos model to the measured MELS data (Figure 6). The best fit parameters, krad = $8.7 \times 10^6\ s^{-1}$, knonrad = $5.6 \times 10^3\ s^{-1}$, kISC = $9.5 \times 10^6\ s^{-1}$, and kRISC = $2.5 \times 10^5\ s^{-1}$ compare reasonably well with previous independent transient PL measurements on bare emitter films as well as with the parameters extracted from transient EL measurements on the same samples (Figure 7). The remarkable agreement between measured and simulated MELS spectrum highlights how well the full dynamic OLED response can be reproduced with the electrooptical model including all relevant physical process ranging from charge injection to exciton decay.

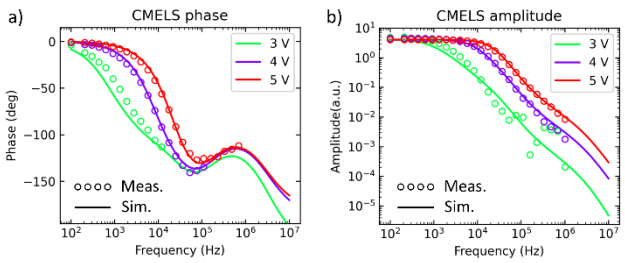

Figure 6. Setfos model fit of the spectral CMELS phase (a) and amplitude (b) for varying bias voltage.

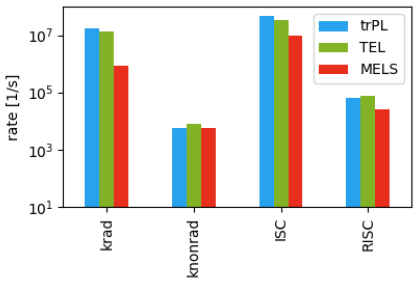

Figure 7. Comparison of exciton parameters extracted from a model fit of the MELS vs. an independent analysis of the transient electroluminescent response (TEL) and from transient PL measurements of a bare emitter film ([4])

3. Degradation analysis

Following the advanced characterization of the fresh devices, we stressed the OLEDs by applying a constant current (15 mA/cm^2), while voltage and emission intensity was continuously monitored, yielding an average lifetime (LT80) of ~8.2 hours. To analyze possible causes of the strong degradation, the continuous lifetime measurement was interrupted in regular time intervals to perform a full steady-state and frequency-domain characterization, yielding additional insight to the change of the charge and exciton dynamics as a function of the operation time.

With the Setfos model we systematically investigated the impact of various potential degradation mechanisms on the JVL, impedance and MELS response, including

- a modification of external contacts (e.g. series resistance)
- the formation of parasitic current pathways (e.g. shunts)
- modification of the charge transport (mobility, charge balance, injection barriers)
- formation of exciton quenching sites
- formation of non-radiative recombination centers.

In particular, a steady decrease in the JV characteristics along with

a significant reduction in the capacitance voltage peak around 3 V and a shift of the MELS amplitude and phase towards lower frequencies was observed, which could be attributed to a reduction in the hole conductivity of the HTL layer (Figure 8). It is worth noting that both a reduction of the hole mobility and the increase of the hole injection barrier at the ITO/MoO_3 contact can equally explain the observed trends in the charge transport and MELS characteristics.

However, the MELS measurements additionally exhibit a decrease of the low-frequency amplitude (red arrow in Fig. 8g) which can directly be linked to the reduction in current efficiency, as the CMELS transfer function is equivalent to the (differential) current efficiency. The measured efficiency decrease cannot be reproduced by modifying the charge transport parameters alone, but indicates the formation of an additional loss channel such as the generation of non-radiative recombination centers (traps) or exciton quenching sites.

Figure 9a) shows the measured time evolution of the current efficiency vs. voltage. Aging induces a significant efficiency decrease at low voltages (above the onset voltage, indicated by (1)). The efficiency roll-off (2), which is dominant in the fresh device at higher voltages, becomes less pronounced with increasing degradation. Various degradation scenarios considered in the Setfos model are shown in Figures 9b-e). While the reduction of the HTL mobility (or equivalently the charge injection) only leads to a slight efficiency reduction above onset, the formation of deep electron traps acting as non-radiative recombination centers in the EML leads to a low voltage efficiency drop, similar to the one observed in the measurement. Noteworthy this characteristic efficiency loss over time can only be reproduced by the formation of SRH recombination centers when these traps in the EML are formed in vicinity of the NBPhen interface. This is in line with the modeled exciton density profile, which shows its maximum towards the NBPhen interface, i.e. this is where the highest energy dissipation is expected. Neither the mobility reduction nor the formation of trapping centers alone can explain the measured efficiency roll-off at higher voltages. Based on the simulation results, the roll-off can however be attributed to an additional exciton quenching process like triplet-triplet-annihilation (TTA, Fig. 9d) or triplet-polaron-quenching (TPQ) on trapped electrons (Fig. 9e), whereas particularly for the case of TPQ we obtained a good qualitative agreement between the measured and modeled current-efficiency characteristics.

4. Conclusions

A detailed analysis of the electro-optical small signal OLED response using impedance spectroscopy and MELS in combination with numerical device modeling has been proven very effective to investigate the interplay of the numerous mechanisms and parameters determining the OLED device characteristics. In particular, we have shown that the essential exciton parameters in TADF emitters can be extracted by a model fit of the MELS response of the full OLED stack. From a systematic characterization during device stressing, we have narrowed down the possible degradation mechanisms and identified TPQ, a reduced hole conductivity and the formation of electron traps in the EML as the dominant processes determining efficiency and lifetime in the investigated samples. The overall excellent agreement between simulated and modeled device characteristics highlights the advantage of full device simulation to design, analyze, and optimize OLEDs.

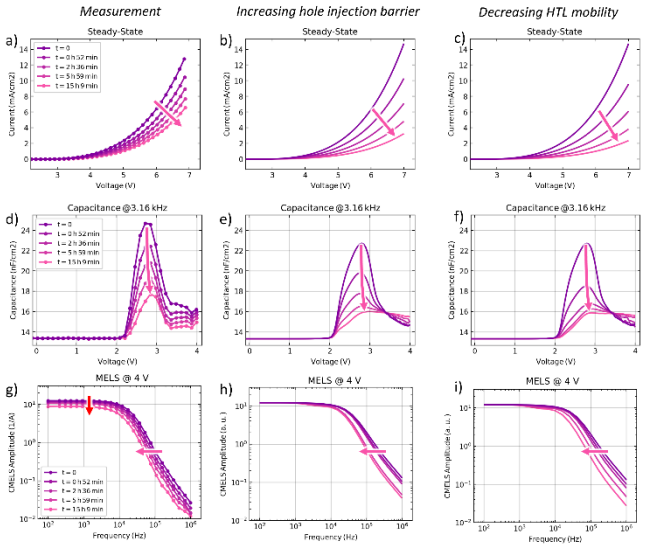

Figure 8. Time evolution of the steady-state JV (a – c), the mid-frequency capacitance-voltage characteristics (d-f) and the CMELS amplitude (g-i) during constant current stressing. The decrease in JV, the lowering of the capacitance peak and the frequency shift of the CMELS response are well reproduced assuming an increasing hole injection barrier or decreasing HTL mobility, but the low frequency reduction of the MELS amplitude (red arrow) is assumed to have a different origin.

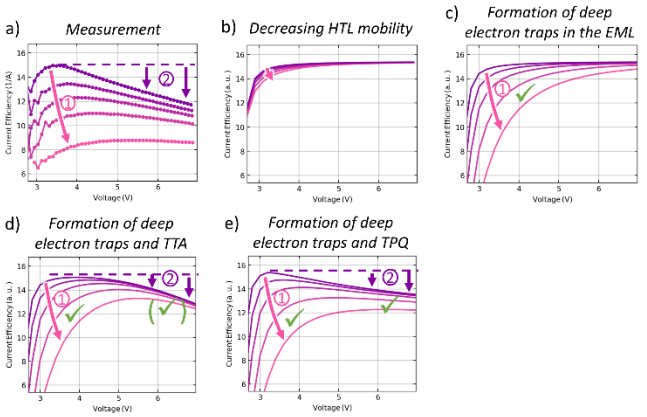

Figure 9. a) Measured time evolution of the current efficiency vs. voltage and the corresponding Setfos model for potential quenching and degradation mechanisms (b – e). A good qualitative agreement is obtained, assuming a continuous increase of deep electron traps in the EML layer in combination with triplet-polaron quenching (TPQ). The latter also reproduces the characteristic efficiency roll-off observed in the fresh device.

5. References

1. S. Nowy, W. Ren, J. Wagner, J. A. Weber, and W. Brütting, Proc. SPIE 7415, (2009)
2. K. Misiakos, J. Park, A. Neugroschel, and F. Lindholm, Solid-State Electronics, 33 (1990)
3. K. Bansal and S. Datta, Journal of Applied Physics, 110(11) 114509 (2011)
4. S. Jenatsch, S. Züfle, B. Blülle, and B. Ruhstaller, Journal of Applied Physics, 127, 031102 (2020)